Collective magnetic properties of cobalt nanocrystals self-assembled in a hexagonal network: Theoretical model supported by experiments

V. Russier, C. Petit, J. Legrand, and M. P. Pileni*
Université Pierre et Marie Curie, Laboratoire SRSI, URA 1662, 4 place Jussieu, 75251 Paris Cedex, France and CEA-Saclay, DSM/DRECAM/SCM, 91191 Gif sur Yvette Cedex, France
(Received 19 August 1999; revised manuscript received 23 December 1999)

Numerical calculations of magnetization curves versus applied field based on a simple model taking into account dipolar interactions were performed for cobalt nanocrystals deposited on a substrate and organized in a hexagonal network. A random distribution of the easy axes orientations of the nanocrystals is considered. The study is focused on the effect of the applied field orientation relative to the substrate surface. Two orientations were chosen: parallel and perpendicular to the surface. The corresponding hysteresis loops are compared to that of a volumic random distribution of nanocrystals at vanishing concentration. The calculation results are compared to experimental data for spherical cobalt nanocrystals coated by lauric acid ($C_{12}H_{25}COO^-$). The particles are either dispersed in hexane (considered as randomly distributed) or deposited in a hexagonal network on a highly oriented pyrolithic graphite substrate. The changes in the magnetization curves with the applied field orientation on the one hand and when going from dispersed to deposited particles on the other hand were calculated and measured. Qualitative agreement is obtained.

I. INTRODUCTION

There is growing interest, both theoretical and experimental, in nanosized magnetic particles.[1] For ferromagnetic materials, different methods are now available to synthesize nanosized Co particles, which are then monodomain magnetic particles.[2–6] It is moreover possible to obtain coated Co particles, which can be either dispersed in a solvent or deposited on a substrate.[2,3] When the particles are deposited on a substrate, self-organized monolayers having a hexagonal structure with more or less large domains free of vacancies can be obtained.[2,3]

There are still points that are not clear in the magnetic properties of such particles, whether these are dispersed in the solvent or assembled in two-dimensional monolayers. One must distinguish the properties depending on the atomic scale structure of the particle[6] from those involving the interactions between particles.[7–19] For coated particles, the distance of closest approach between particles is expected to be large enough for the interactions to have mainly a magnetostatic character. Then the comparison of the magnetic properties of particles dispersed in the solvent to those of particles deposited on a substrate provides a relevant method for estimating the magnitude of magnetostatic interactions between particles.

Numerical simulations of the influence of the dipolar interactions between ferromagnetic particles on the magnetic properties have been performed.[12–14] These simulations concern homogeneous and isotropic three-dimensional dispersions of ferromagnetic and spherical particles, with randomly distributed easy axes. The dipolar interactions have been already investigated through the magnetization curves for thin films including ferromagnetic particles such as CoCr (Refs. 15 and 16) or CoCrPt (Ref. 17) films, where the magnetic anisotropy is strongly oriented in the direction normal to the film surface. The difference between the magnetization curves corresponding to the applied field normal and parallel to the surface is mainly determined by the degree of orientation of the magnetic anisotropy. A two-dimensional random field Ising model[18] including dipolar interactions, adapted to this kind of situation, has been developed. An increase in the dipolar interactions when the field is normal to the surface leads to a tilt of the hysteresis loop and a decrease in the remanence magnetization. Recently,[19] the magnetic properties of Co bilayer islands deposited on a Au(111) surface have been studied both experimentally and theoretically. In the latter case, the particles interact through exchange interactions which behave conversely to the dipolar interactions, when the applied field is normal to the surface, at least in high applied field situations.

In this paper, we focus on the dipolar interactions between cobalt nanocrystals, characterized by a random distribution of the easy axes and deposited on graphite. The hysteresis loop at very low temperature (3 K) is investigated both experimentally and theoretically. Cobalt nanoparticles are synthesized by using the reverse micelle technique,[20] from which coated cobalt nanocrystals with 6-nm average diameter are obtained.[2,3] The magnetization curves for the particles dispersed in a solvent or deposited on the graphite substrate are measured. In the latter case, the orientation of the external field with respect to the substrate surface plays an important role. Hence, the comparison of the hysteresis loop recorded with the field either parallel or normal to the substrate leads to an estimation of the effect of the dipolar interactions. Computations are made using a simple model including the elements required to determine the hysteresis loop by taking into account the dipolar interactions between particles. The particles are modeled as Stoner-Wohlfarth particles[21,22] and an important simplification is made: only the component parallel to the applied field of the total dipolar field is taken into account. This enables us to include a large number of sites in the calculation of the long-range dipolar field. The ratio of the remanence magnetization correspond-

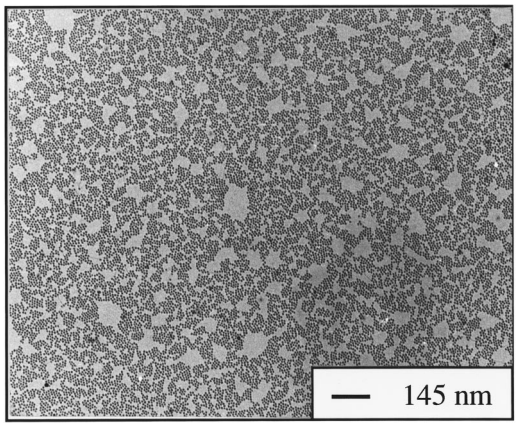

FIG. 1. TEM pattern of cobalt nanoparticles at different magnifications after deposition on amorphous carbon.

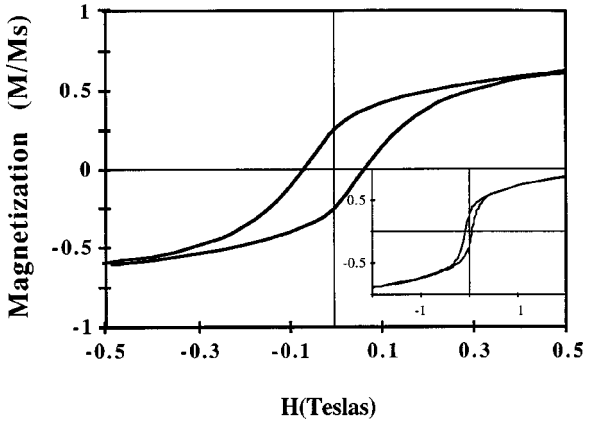

FIG. 2. Experimental hysteresis curve at 3 K for the particles dispersed in the solvent (0.01% in volume in hexane). The inset shows the behavior at high field up to 2 T.

ing to the applied field normal and parallel to the surface, respectively, is found to be a relevant measure of the dipolar interactions. Good agreement between the experimental and the calculated data is obtained.

II. EXPERIMENTAL RESULTS

A. Synthesis and characterization of cobalt nanoparticles

The synthesis of cobalt nanoparticles, using reverse micelles (water in oil droplets) as microreactors,[20] has been described in our previous papers.[2,3] These particles are obtained by mixing two micellar solutions characterized by the same droplet diameter (3 nm): the first contains 10^{-2} M $Co(AOT)_2$ [cobalt bis(2 ethyl-hexyl) sulfosuccinate] and the second 2×10^{-2} M sodium tetrahydroboride ($NaBH_4$). After mixing, the micellar solution remains optically clear. Its color turns immediately from pink to black, indicating formation of colloidal particles. The particles are highly dispersed and no aggregation occurs. They are extracted from reverse micelles under anaerobic conditions by covalent attachment of lauric acid and then redispersed in hexane. This chemical treatment highly improves the stability of cobalt nanoparticles exposed to air. Nanoparticles have been characterized by x-ray diffraction and small-angle x-ray scattering. From these analyses it is concluded that nanocrystals are spherical (to a very good approximation) and consist of metallic fcc cobalt.[3] With these techniques, it has not been possible to detect any external layers of cobalt derivatives.

Deposition of a drop of solution on a carbon grid leads to a large coverage of the substrate by the particles (Fig. 1). Locally the nanocrystals are arranged in a hexagonal network; their average size is 5.8 nm and the dispersion in the size distribution is about 11%.

B. Magnetic properties of cobalt

The zero-field-cooled and field-cooled (ZFC/FC) curves are recorded with a field of 75 Oe. The FC curve shows a uniform decay, which confirms the superparamagnetic behavior at high temperature. The ZFC curve shows a pronounced peak at 60 K at the blocking temperature, T_b. Using the average particle volume determined by transmission electron microscopy (TEM), the evaluated anisotropy constant is 2.5×10^6 erg/cm^3. This value is similar to that observed in the bulk phase. This is rather surprising. In fact, there is clear evidence in the literature that the anisotropy constant markedly increases with decreasing particle size.[23–26] Klabunde *et al.*[4] determined the anisotropy constant for cobalt nanoparticles smaller than those described here and their value is not greatly different from ours. For cobalt nanocrystals with 4.5-nm average diameter they found an anisotropy constant twice that obtained for the bulk phase. Furthermore, by interpolation of data given in Ref. 4, an anisotropy constant around 3×10^6 to 3.5×10^6 ergs/cm^3 is deduced for 6-nm nanocrystals. This value is the same order of magnitude as that deduced from the ZFC magnetization curve. TEM shows that the nanocrystals are spherical, thus to a first approximation shape anisotropy can be excluded.

At 3 K, the nanocrystals are ferromagnetic. The magnetization curves are recorded for nanoparticles dispersed in hexane (Fig. 2) and deposited on a graphite substrate (Fig. 3). When 0.01% volume fraction of nanocrystals is dispersed in hexane, the saturation magnetization, M_s, is not reached at 2 T but from extrapolation of the plot of M/H versus H, M_s is 110 emu/g, which is significantly lower than the value of bulk fcc cobalt, $M_s(\text{bulk})=162$ emu/g. The ratio of remanence to saturation magnetization is 0.25. The large difference between the saturation magnetization of nanocrystals, M_s, and that of the bulk phase, $M_s(\text{bulk})$, is attributed to the strong interactions between the carbonyl group of the coating agent and the cobalt atoms at the particle surface. This is supported by the fact that adsorbed species on metal magnetic nanocrystals change the magnetization of the particles through the quenching of the surface atom contribution.[23,24,27] This was calculated and observed for small nickel and NiPt clusters ($Ni_{38}Pt_6$) coated by CO ligands. Carbonyl ligands completely quench the magnetic moments of the nickel atoms at the cluster surface, leaving the inner-core metal atoms unaffected.[27]

Magnetization curves for particles deposited on the substrate and submitted to fields either parallel or perpendicular to the substrate surface are shown in Figs. 3(a) and 3(b), respectively. Figure 3 shows clearly the change in the shape of the hysteresis loop with the orientation of the applied field relative to the substrate surface. When the field is parallel to the surface, the remanence to saturation magnetization ratio is 0.28 and the hysteresis loop is squarer than that corre-

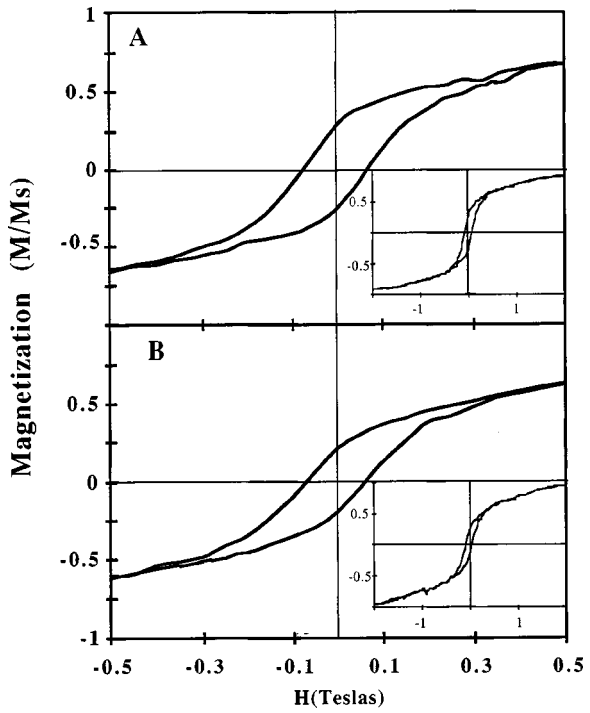

FIG. 3. Experimental hysteresis curves at 3 K for the particles deposited on the graphite substrate (HOPG). The inset shows the saturation behavior at high field up to 2 T. (a) applied field parallel to the surface; (b) applied field normal to the surface.

sponding to the particles dispersed in solution. Conversely, when the field is perpendicular to the surface, the hysteresis loop is smoother than that corresponding to the dispersed particles and the remanence to saturation magnetization ratio is 0.21. For the two orientations of the field, saturation is reached at 2 T, and the saturation magnetization value M_s is 110 emu/g. Moreover, the coercive field H_{co} has the same value in all cases, $H_{co}=0.07$ T.

III. NUMERICAL CALCULATIONS

The purpose of the numerical calculations is to examine the influence on the magnetization curves of the dipolar magnetostatic interactions between the cobalt nanocrystals. The magnetization in the direction of the applied field is calculated. The monolayer is modeled by an assembly of spherical particles with uniaxial anisotropy, located at the sites (labeled k) of a perfect two-dimensional lattice with either a hexagonal or square structure. The surface plane is the $(\hat{x},\hat{y})$ plane, the normal to the surface is the $\hat{z}$ axis, and the applied field is either normal or parallel to the surface plane. No thermal effect is included since we focus on the very low temperature limit (3 K) of the hysteresis loop. To simplify, a monodisperse system is considered (the dispersion in the size distribution, which is evaluated at 11% in the experimental samples, is neglected). Since on the one hand the system was frozen at zero field, and on the other hand the particles exhibit a superparamagnetic behavior at the freezing temperature of the solvent (230 K), the easy axes, $\hat{n}_k$, are randomly distributed over a unit sphere. This model enables switching the interaction: this noninteracting system corresponds to the particles dispersed in the solvent at vanishing concentration.

For the monolayer the interaction must be taken into account. The particles are modeled as Stoner-Wohlfarth particles[21,22] characterized by an anisotropy constant K, a bulk saturation magnetization M_s, and a volume $v_0=(\pi/6)D^3$, where D is the particle diameter. The only interaction between the particles is the classical dipolar interaction. Therefore, the energy of a particle located at site k is given by

$$E_k=-Kv_0(\hat{n}_k\cdot\mu_k)^2-\mathbf{H}_{\rm eff}(k)\cdot\hat{\mu}_k, \tag{1}$$

where $\mathbf{H}_{\rm eff}(k)$ and $\boldsymbol{\mu}_k=M_s v_0\hat{\mu}_k$ are the effective magnetic field felt by the particle and the magnetic moment of the particle, respectively. Here and in the following, circumflexes denote unit vectors. For symmetry reasons,[21,22] the equilibrium position of the moment belongs to the plane defined by the unit vectors $\hat{n}_k$ and $\hat{H}_{\rm eff}(k)$ and Eq. (1) can be rewritten

$$E_k=-Kv_0(\hat{n}_k\cdot\hat{\mu}_k)^2-H_{\rm eff}(k)\cdot\mu_k\cos(\psi_k-\theta_k), \tag{2}$$

where Ψ_k and Θ_k are the angles $[\hat{n}_k,\hat{H}_{\rm eff}(k)]$ and $(\hat{n}_k,\hat{\mu}_k)$, respectively. The effective magnetic field at site k is the sum of the applied field, $\mathbf{H}_a$ and the total dipolar field:

$$H_{\rm eff}(k)=\mathbf{H}_a+\frac{\mu}{d^3}\sum_{j\neq k}\frac{3(\hat{\mu}_j\cdot\hat{r}_{jk})\hat{r}_{jk}-\hat{\mu}_j}{(r_{jk}/d)^3}$$

$$\equiv\mathbf{H}_a+\frac{\mu}{d^3}\sum_{j\neq k}\mathbf{h}_{\rm dip}(jk), \tag{3}$$

where $\hat{r}_{jk}$ is the unit vector in the direction joining particles j and k, and d is the nearest-neighbor distance. For convenience we introduce reduced fields

$$\mathbf{H}_{\rm eff}(k)=H_K\left(\mathbf{h}_a+\alpha_d\sum_{j\neq k}\mathbf{h}_{\rm dip}(jk)\right)\equiv H_K[\mathbf{h}_{\rm eff}(k)], \tag{4}$$

where $H_K=(2Kv_0/\mu)=(2K/M_s)$ is the usual anisotropy field, $\mathbf{h}_{\rm dip}(j,k)$ is defined by Eq. (3), and the coupling constant α_d is given by

$$\alpha_d=\frac{\pi}{12}\frac{M_S^2}{K}(D/d)^3. \tag{5}$$

The configuration of the magnetic moment orientations $\{\hat{\mu}_k\}$ is determined from the minimization of the total energy of the system. This is done first by setting $\hat{\mu}_k$ in the plane defined by $\hat{h}_{\rm eff}(k)$ and $\hat{n}_k$, and then by determining the angle Θ_k from the local equilibrium condition[21,22]

$$\frac{\partial E_k}{\partial\Theta_k}=0,\quad \frac{\partial^2 E_k}{\partial\Theta_k^2}>0. \tag{6}$$

According to the value of the effective field and to the characteristics of the Stoner-Wohlfarth particle at site k, this leads either to one or two solutions, $\Theta^{(u)}$ and $\Theta^{(d)}$ corresponding to the ''up'' and ''down'' states, respectively. In other words, the local magnetization at site k in the direction of the effective magnetic field $\mathbf{h}_{\rm eff}(k)$ follows the hysteresis loop of the corresponding Stoner-Wohlfarth particle. This energy minimization leads to metastable equilibrium states, since we do not consider thermal activation. As a result, each

particle may be found in either the up or the down state, according to the value of the effective field and the history of the system (i.e., the complete set of consecutive configurations of the system driven by the applied field). This method is equivalent to obtaining the infinite time limit of the moments from the Landau-Lifshitz-Gilbert equation[28] in the large damping limit. This is currently used for the calculation of hysteresis loops.[29–31] Similarly, in their Monte Carlo simulation of the hysteresis loop, Anderson *et al.*[12] impose that the moments of the particles stay in the direction of one of the minima.

Due to the long-range character of dipolar fields [Eq. (3)], a large number of sites have to be taken into account in the calculation. For this, and in order to limit the computation time, the description is simplified by taking into account, at each site k, only the contribution to the dipolar fields $\mathbf{h}_{\rm dip}(j,k)$ due to the component in the direction of the applied field $\mathbf{h}_a$ of the moment $\boldsymbol{\mu}_j$. When the applied field is normal to the surface plane, this is equivalent to considering only the contribution in the direction of the applied field of the total dipolar field. When the applied field is in the surface plane, say in the $\hat{x}$ direction, the contribution to the dipolar field, $h_{\rm dip}(j,k)$, due to the $\hat{y}$ component of the moments $\boldsymbol{\mu}_j$ is also neglected. This approximation is justified by the angular dependence of the dipolar field and by the symmetries of the system (a well-ordered lattice and randomly distributed easy axes). A second justification of our approximation is that we focus on the sum of the local magnetizations in the direction of the applied field,

$$M(h_a)=\frac{1}{N_s}\sum_k \hat{\mu}_k\cdot\hat{h}_a\equiv\frac{1}{N_s}\sum_k m_k, \tag{7}$$

which is a property averaged over all the sites. This does not mean that all the moments are either parallel or antiparallel to the applied field, but only that the net result of the contributions to the total dipolar field of the components normal to the applied field of the moments vanishes. Therefore, concerning the orientations of the magnetic moments, we go beyond the dipolar Ising model introduced in Ref. 18, where $m_k=\pm 1$. As we shall see, this allows us to treat a large number of sites avoiding the introduction of a cutoff radius.[12,13]

In the framework of this model, the effective field is in the direction of the applied field, $\mathbf{h}_{\rm eff}(k)=h_{\rm eff}(k)\hat{h}_a$, and as a result the angles Ψ_k take constant values when the magnitude of the applied field varies. Thus, each lattice site is characterized by a scalar variable, $m_k=\mu_k(\hat{\mu}_k\cdot\hat{h}_a)$, depending on the magnitude of the effective field, $h_{\rm eff}(k)$. Therefore, we have

$$m_k(\varphi_k)=\cos(\Theta_k(h_{\rm eff}(k),\Psi_k,\varphi_k)), \tag{8a}$$

$$h_{\rm eff}(k)=h_a-\alpha_d\sum_{j\neq k}\frac{m_j}{(r_{jk}/d)^3}\quad\text{for }\hat{h}_a=\hat{z}, \tag{8b}$$

$$h_{\rm eff}(k)=h_a+\alpha_d\sum_{j\neq k}\frac{3m_j(x_{jk}^2-1)}{(r_{jk}/d)^3}\quad\text{for }\hat{h}_a=\hat{x}, \tag{8c}$$

where Θ_k is determined from Eq. (6) and the variable φ_k describes the state of the particle ($\varphi_k=+1$ or -1 for the up and down states, respectively). The calculation is performed on a grid including N_s sites. The long-range character of the dipolar field is accounted for by considering eight neighboring grids deduced from the original one by periodicity.

In order to reduce the computing time, the solutions of Eq. (6), which involves a Newton-Raphson routine, are not calculated each time. Instead, first we discretize the variable Ψ by considering a finite number, N_Ψ of values of Ψ. For each of these, Eq. (6) is solved once for a set of values of the field $\{h_{n=1,Nh}\}$. This set of values depends strongly on the corresponding value of Ψ as it takes into account the discontinuities of the solutions $\Theta^{(u,d)}(h)$ of Eq. (6) at the critical fields $\pm h_c(\Psi)$. Typically, we use $N_\Psi\geqslant 10$ and $N_h\geqslant 40$. Then, $\Theta^{(u,d)}(h_{\rm eff}(k))$ is obtained by an interpolation from the array of calculated values, $\Theta^{(u,d)}(h_n,\Psi_i)$ up to second order in the derivation $[h_{\rm eff}(k)-h_n]$.

Two different numerical schemes have been considered, corresponding to two different starting configurations of the moments.

(i) A totally saturated state, where $m_k=+1$ for all k, is the starting point. Thus the component of the dipolar field in the applied field direction takes the same value on all the sites. For an infinite lattice we have

$$\sum_{j\neq k}h_{\rm dip}(jk)=-\sum_{j\neq k}\frac{1}{(r_{jk}/d)^3}=-S_z\quad\text{for }\hat{h}_a=\hat{z}$$

and

$$m_k=1,\quad\forall k, \tag{9a}$$

$$\sum_{j\neq k}h_{\rm dip}(jk)=-\sum_{j\neq k}\frac{1-3(x_{jk}^2)}{(r_{jk}/d)^3}=\tfrac{1}{2}S_z\quad\text{for }\hat{h}_a=\hat{x}$$

and

$$m_k=1,\quad\forall k, \tag{9b}$$

with $S_z=9.033\,62$ and $11.034\,17$ for the square and the hexagonal lattice, respectively. The second equality in Eq. (9b) follows from the symmetry of the lattices that are considered. Then the magnitude of the applied field decreases, all the sites are examined in a random order, and the corresponding m_k values are determined by Eqs. (8). After each variation of the value of a projected moment, say m_{ko} at site k_o, the dipolar fields at all the sites $k\neq k_o$ are updated. The process is performed iteratively until the maximum deviation of the m_k from their equilibrium value is less than a threshold value, $\varepsilon=10^{-3}$. Finally the total magnetization per site, normalized by the saturation magnetization M_s in terms of the applied field, is determined according to Eq. (7).

(ii) Starting from a totally demagnetized state makes it possible to determine the first magnetization curve. In this case, the starting point is obtained by choosing randomly one-half of the N_s sites which are set in the ''down'' state, the other ones being in the ''up'' state. The initial values of both the total dipolar field and of m_k at each site are zero. The first point, corresponding to $H_a=0$, is obtained by iteratively calculating the values of the total dipolar field and of the magnetization m_k in a self-consistent way as outlined above. After the determination of the configuration corresponding to $H_a=0$ and $M(H_a=0)=0$, the procedure out-

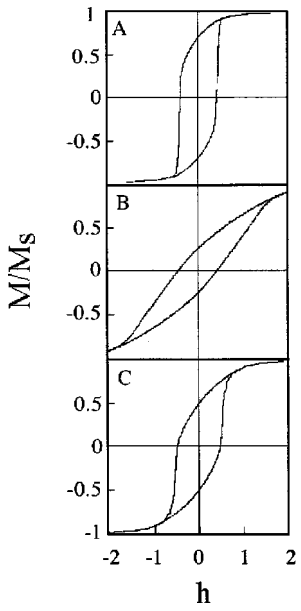

FIG. 4. Calculated hysteresis curves for the hexagonal lattice. (a) $\alpha_d=0.10$ and the applied field is parallel to the surface; (b) $\alpha_d=0.10$ and the applied field is normal to the surface; (c) noninteracting particles ($\alpha_d=0$), corresponding to the disperesd particles at vanishing concentration.

lined above is followed while the applied field increases to reach the totally saturated state, $M(H_a)=1.0$. Then, the total cycle is calculated. From this second scheme, beside the determination of the first magnetization curve, we can compute the hysteresis loop when some of the lattice sites are unoccupied, since then Eqs. (9) do not hold as the starting point. This corresponds to the case of a nonperfect monolayer of particles (as shown on Fig. 1).

IV. RESULTS AND DISCUSSION

A. Results of the model

The parameters needed to deduce the value of the coupling constant α_d involved in the calculation are the characteristics of the nanocrystal material, namely the anisotropy constant K, the saturation magnetization M_s, the particle diameter D, and the nearest-neighbor distance d. In the first step the expected range of variation of α_d is determined for a monolayer of spherical cobalt particles. The maximum value of α_d is obtained by using the characteristic of cobalt fcc bulk material. The anisotropy constant and the saturation magnetization are 2.5×10^6 ergs/cm^3 and 162 emu/g, respectively. This leads to $\alpha_d=0.2118(D/d)^3$. For our system, the average size, D, is in the range 5–7 nm and the corresponding nearest-neighbor distance, d, is in the range 7–9 nm. Then the calculated α_d is in between 0.075 and 0.10. Hence, the maximum value for the coupling constant of the monolayer made of coated cobalt nanocrystals is $\alpha_d\approx0.10$. Thus calculations have been performed for α_d between 0.03 and 0.10.

All the calculations are performed with $N_s=2500$ sites, $N_\Psi=12$, and $N_h=43$. These N_Ψ and N_h values are sufficient to obtain very accurate results from the interpolation scheme. The hysteresis loops corresponding to $\alpha_d=0.10$ and the two orientations of the applied field are shown in Figs. 4(a) and 4(b). The noninteracting case, $\alpha_d=0$, corresponding to dispersed particles is also shown [Fig. 4(c)]. At a qualitative level, the hysteresis loop is sharper than that corresponding to the isolated particles ($\alpha_d=0$) when the applied field is parallel to the surface. Conversely, it is smoother and tilted when the applied field is normal to the surface. The nanocrystals are not close enough to reach a coercivity due to dipolar interactions alone. The hysteresis loops calculated for the square and the hexagonal lattices with the same value of α_d are very close. Therefore, the lattice structure has a negligible effect on the magnitude of the deviation of the magnetization due to dipolar interactions. The coupling constant α_d (and thus the packing fraction of the monolayer) appears to be the major parameter for this deviation.

In order to take into account the presence of vacancies observed in the experimental samples, calculations are performed by introducing a fraction, f_d, in the lattice of unoccupied sites chosen randomly. The f_d effect (for $f_d\leqslant0.40$) is very well reproduced by introducting an effective coupling constant given by

$$\alpha_{\text{eff}}=\alpha_d(1-f_d^x) \quad \text{with} \quad x=1.15. \tag{10}$$

In other words, the hysteresis loop corresponding to a given α_d value and $f_d\neq0$ coincides with that corresponding to $\alpha_d=\alpha_{\text{eff}}(\alpha_d,f_d)$ and $f_d=0$. Thus, at least for small f_d values, the presence of vacancies in the experimental samples will be taken into account by reducing the coupling constant α_d. A crude estimation of the effect of f_d when $f_d\to0$ can be obtained by considering that the unoccupied sites are uniformly distributed and form a sublattice. The lattice spacing of this sublattice of unoccupied sites is $d_u=d/f_d^{1/2}$. Following a mean-field-like reasoning, we assume that all the occupied sites are equivalent (i.e., are characterized by the same value of the projected moment in the direction of the field, m_k). Then, on a given site k, the sum of all the dipolar fields due to the occupied sites, $j\neq k$, is the sum of all the dipolar fields due to the moments m_k located on all the sites from which one subtracts the sum of the dipolar fields due to the moments m_k located on the sites of the sublattice of unoccupied sites. The sum of dipolar fields of equal-valued moments located on a regular two-dimensional lattice varies as $(1/d)^3\propto\alpha_d$ and therefore we get, when $f_d\to0$, $\alpha_{\text{eff}}=\alpha_d[1-(d/d_u)^3]=\alpha_d(1-f_d^{3/2})$, which coincides with Eq. (10) with $x=\frac{3}{2}$.

In order to estimate quantitatively the effect of the dipolar interactions on the magnetization of the system, the remanence magnetization when the applied field is either parallel, $M_r^{\parallel}$, or normal $M_r^{\perp}$, to the substrate is calculated in terms of the coupling constant, α_d [Fig. 5(a)]. The ratio $\gamma=M_r^{\perp}/M_r^{\parallel}$ appears to be the relevant variable to test the magnitude of the dipolar interactions since it is expected to depend mainly on the value of the coupling constant α_d and not on the hysteresis loop shape. The variation of γ with α_d is shown in Fig. 5(b).

B. Comparison between the model and the experiments

The quantitative comparison between the model and the experimental data is presented in this section. Instead of using the parameter given for the bulk material, we use those

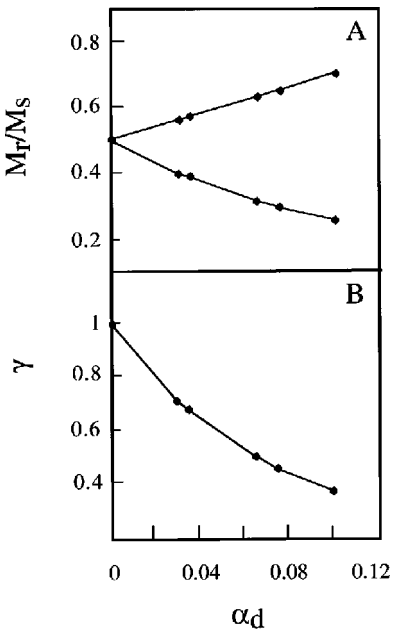

FIG. 5. (a) Remanence magnetization M_r/M_s calculated in terms of α_d. The upper and lower curves correspond to the applied field parallel and normal to the surface, respectively. The lines are guides for easier visualization. (b) Ratio $\gamma=[M_r^{\perp}/M_r^{\parallel}]$ in terms of α_d.

determined from the experiments. The anisotropy constant, deduced from ZFC magnetization measurement, is 2.5×10^6 ergs/cm^3. As already discussed above, this value is similar to that of the bulk phase[32,33] and is the same order of magnitude as that extrapolated to 6 nm from data obtained by other groups.[4] The saturation magnetization is also deduced from magnetization curves ($M_s=110$ emu/g). This value is low compared to that expected and is attributed, as stated above, to a chemisorption process.

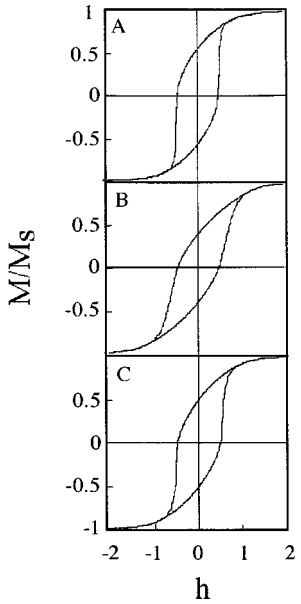

FIG. 6. Calculated hysteresis on hexagonal lattices. (a) $\alpha_d=0.03$, applied field parallel to the surface; (b) $\alpha_d=0.03$, applied field normal to the surface; (c) $\alpha_d=0$, case of isolated particles.

At the quantitative level, it is impossible to compare the hysteresis loop deduced from the model to that obtained experimentally. This is due to the fact that the shapes of these two curves differ markedly, which is a result of the rough approximation of the model. As a matter of fact, the approximation made by using an assembly of Stoner-Wohlfarth involves one given spin orientation. With nanocrystals, because of the surface spin canting, several spin orientations occur. This induces an increase in the magnetization far above the hysteresis loop. As observed in Fig. 2, the saturation magnetization increases with the applied field. Saturation is reached at a rather large field. Conversely, the model predicts that a saturation magnetization is reached immediately. The measured coercive field ($H_{co}\approx0.07$ T) is very low compared to that calculated ($H_{co}=0.252$ T) for a saturation magnetization of 110 emu/g. However, some quantitative comparisons are made. The effective coupling constant, α_d, is calculated taking into account the average diameter of the particle ($D=6$ nm) and the nearest-neighbor distance ($d=8.5$ nm). This leads to a coupling constant α_d of 0.035. Assuming a fraction of vacancies of approximately $f_d=0.20$, the effective coupling constant [Eq. (10)] is 0.030. The corresponding hysteresis curve is shown in Fig. 6. From Fig. 5(b), the ratio γ, corresponding to $\alpha_d=0.030$, is $\gamma\approx0.70$. This calculated value is compared to that deduced from the experimental measurements. As a matter of fact, the reduced remanences measured when the applied field is perpendicular and parallel to the substrate are 0.21 and 0.28, respectively. The experimental value of γ is then $\gamma^{\mathrm{exp}}=M_r^{\perp}/M_r^{\parallel}=0.75\pm0.08$. This value is in good agreement with that determined from the model ($\gamma=0.70$). It is important to note that these reduced remanences ($M_r^{\perp}$ and $M_r^{\parallel}$) are measured by using the same sample with the same saturation magnetization (it does not depend on the applied field orientation). This suppresses errors in the saturation magnetization. The good agreement between experimental and theoretical data enables us to conclude that the change in the hysteresis loops with the applied field orientation is due to dipolar interactions between nanocrystals. As mentioned in the model, at a fixed α_d value, no drastic changes are observed with the lattice geometry. This leads to the conclusion that the change in the magnetization curves of nanocrystals either deposited on a substrate or dispersed in a matrix is mainly due to the high ''local'' concentration of nanocrystals. On a substrate, the close vicinity of the magnetic moments favors collective magnetic dipole-dipole interactions. From experimental measurements and calculations, it is shown that the coercive field of nanocrystals deposited on a substrate does not markedly depend on the applied field orientation and is very close to that observed for isolated particles. The very weak variation of the coercive field is due to the low coupling constant. Furthermore, the calculations lead to a linear behavior for $[h_{co}(\alpha_d)/h_{co}(0)]$ with respect to α_d, with a slope close to -1.5. This implies a deviation not larger than 5% between the coercive field of the dispersed and deposited particles, respectively. The order of magnitude obtained from the present calculations is comparable to those given in Refs. 13 and 14, where three-dimensional systems are considered. The fact that h_{co} is independent of the field orientation may be due in a large part to the random distribution of the easy axes.

V. CONCLUSION

In this work, the hysteresis curve of two-dimensional self-organized monolayers of cobalt nanocrystals, determined both experimentally and theoretically, is presented. A change in the shape of the hysteresis loop with the applied field orientation relative to the sample surface is observed. The model used for the numerical calculations is to be understood as a minimum model, which nevertheless includes the necessary elements for the investigation of the dipolar interactions. The approximations make it possible to include a large number of sites in the calculation of the dipolar field. This is necessary because of the long-range character of the dipole-dipole interaction: in a 2D system, the sum of the dipolar fields behaves as $1/N^{1/2}$, where N is the total number of sites taken into account. From the calculated hysteresis loops, we conclude that the difference between the hysteresis curves measured with an applied field parallel or normal to the sample surface is mainly due to the dipolar interactions between particles. This is a direct consequence of the random distribution of the easy axes of the particles and this is an important feature of our system. Furthermore, we conclude that the precise structure of the lattice is likely to play only a negligible role. The comparison between the experimental and the numerical results can be done through the ratio γ of the remanence magnetization, as measured with the applied field normal and parallel to the sample surface, respectively. For γ we obtain satisfactory agreement between the calculated and the experimental results.

*Electronic mail: pileni@sri.jussieu.fr

[1] J. L. Dormann, D. Fiorani, and E. Tronc, Adv. Chem. Phys. **98**, 283 (1997).
[2] C. Petit, A. Taleb, and M. P. Pileni, Adv. Mater. **10**, 259 (1998).
[3] C. Petit, A. Taleb, and M. P. Pileni, J. Phys. Chem. B **103**, 1805 (1999).
[4] J. P. Chen, C. M. Sorensen, K. J. Klabunde, and G. C. Hadjanayis, Phys. Rev. B **51**, 11 527 (1995).
[5] X. M. Lin, C. M. Sorensen, K. J. Klabunde, and G. C. Hadjipanayis, Langmuir **14**, 7140 (1998).
[6] M. Respaud, J. M. Broto, H. Rakoto, A. Fert, L. Thomas, B. Barbara, M. Verelst, E. Snoeck, P. Lecante, A. Mosset, J. Ossuna, T. Ould Ely, C. Amiens, and B. Chaudret, Phys. Rev. B **57**, 2925 (1998).
[7] J. L. Dormann, L. Spinu, E. Tronc, J. P. Jolivet, F. Lucari, F. D'Orazio, and D. Fiorani, J. Magn. Magn. Mater. **183**, L255 (1998).
[8] J. L. Dormann, R. Cherkaoui, L. Spinu, M. Noguès, F. Lucari, F. D'Orazio, D. Fiorani, A. Garcia, E. Tronc, and J. P. Jolivet, J. Magn. Magn. Mater. **187**, L139 (1998).
[9] M. El-Hilo, K. O'Grady, and R. W. Chantrell, J. Magn. Magn. Mater. **114**, 295 (1992).
[10] S. Mørup and E. Tronc, Phys. Rev. Lett. **72**, 3278 (1994).
[11] J. L. Dormann, L. Bessais, and D. Fiorani, J. Phys. C **21**, 2015 (1981).
[12] J. O. Andersson, C. Djurberg, T. Jonsson, P. Svedlindh, and P. Nordblad, Phys. Rev. B **56**, 13 983 (1997).
[13] M. El-Hilo, R. W. Chantrell, and K. O'Grady, J. Appl. Phys. **84**, 5114 (1998).
[14] D. Kechrakos and K. N. Trohidou, Phys. Rev. B **58**, 12 169 (1998).
[15] J. G. Zhu and H. N. Bertram, J. Appl. Phys. **66**, 1291 (1989).
[16] G. Bottoni, D. Candolfo, and A. Cecchetti, J. Appl. Phys. **85**, 4729 (1999).
[17] C. Haginoya, S. Heike, M. Ishibashi, K. Nakamura, and K. Koike, J. Appl. Phys. **85**, 8327 (1999).
[18] A. Magni, Phys. Rev. B **59**, 985 (1999).
[19] S. Padovani, I. Chado, F. Scheurrer, and J. P. Bucher, Phys. Rev. B **59**, 11 887 (1999).
[20] M. P. Pileni, J. Phys. Chem. **97**, 6961 (1993).
[21] E. C. Stoner and E. P. Wohlfarth, Philos. Trans. R. Soc. London, Ser. A **240**, 599 (1948); reprinted in IEEE Trans. Magn. **27**, 3475 (1991).
[22] H. Pfeiffer, Phys. Status Solidi A **122**, 377 (1990).
[23] F. Bøker, S. Mørup, and S. Linderoth, Phys. Rev. Lett. **72**, 282 (1994).
[24] G. M. Pastor, J. Dorantes-Dávila, S. Pick, and H. Dreyssé, Phys. Rev. Lett. **75**, 326 (1995).
[25] P. Bruno, Phys. Rev. B **39**, 865 (1989).
[26] D. S. Wang, R. Wu, and A. J. Freeman, Phys. Rev. Lett. **70**, 869 (1993).
[27] D. A. van Leeuwen, J. M. Van Ruitenbeck, L. J. de Jongh, A. Ceriotti, G. Pachioni, O. D. Häberlen, and N. Rösch, Phys. Rev. Lett. **73**, 1432 (1994).
[28] W. F. Brown, Phys. Rev. **130**, 1677 (1963).
[29] R. Ferré, B. Barbara, D. Fruchart, and P. Wolfers, J. Magn. Magn. Mater. **140–144**, 385 (1985).
[30] D. A. Dimitrov and G. M. Wysin, Phys. Rev. B **50**, 3077 (1994); **51**, 11 947 (1995).
[31] R. H. Kodama and A. E. Berkowitz, Phys. Rev. B **59**, 6321 (1999).
[32] W. Sucksmith and J. E. Thompson, Proc. R. Soc. London **225**, 362 (1954).
[33] W. D. Doyle and P. J. Flanders, in *Proceedings of the International Conference on Magnetism, Nottingham, 1964* (The Institute of Physics and the Physical Society, Bristol, 1965).